

Article

# Strong Photoluminescence Enhancement from Bilayer Molybdenum Disulfide via the Combination of UV Irradiation and Superacid Molecular Treatment

Yuki Yamada, Takeshi Yoshimura, Atsushi Ashida , Norifumi Fujimura and Daisuke Kiriya \* 

Department of Physics and Electronics, Osaka Prefecture University, 1-1 Gakuen-cho, Naka-ku, Sakai-shi, Osaka 599-8531, Japan; yamada-07@pe.osakafu-u.ac.jp (Y.Y.); tyoshi@pe.osakafu-u.ac.jp (T.Y.); ashida@pe.osakafu-u.ac.jp (A.A.); fujim@pe.osakafu-u.ac.jp (N.F.)

\* Correspondence: kiriya@pe.osakafu-u.ac.jp

**Abstract:** A direct band gap nature in semiconducting materials makes them useful for optical devices due to the strong absorption of photons and their luminescence properties. Monolayer transition metal dichalcogenides (TMDCs) have received significant attention as direct band gap semiconductors and a platform for optical applications and physics. However, bilayer or thicker layered samples exhibit an indirect band gap. Here, we propose a method that converts the indirect band gap nature of bilayer MoS<sub>2</sub>, one of the representative TMDCs, to a direct band gap nature and enhances the photoluminescence (PL) intensity of bilayer MoS<sub>2</sub> dramatically. The procedure combines UV irradiation with superacid molecular treatment on bilayer MoS<sub>2</sub>. UV irradiation induces the conversion of the PL property with an indirect band gap to a direct band gap situation in bilayer MoS<sub>2</sub> when the interaction between the top and bottom layers is weakened by a sort of misalignment between them. Furthermore, the additional post-superacid treatment dramatically enhances the PL intensity of bilayer MoS<sub>2</sub> by a factor of 700×. However, this procedure is not effective for a conventional bilayer sample, which shows no PL enhancement. From these results, the separated top layer would show a strong PL from the superacid treatment. The monolayer-like top layer is physically separated from the substrate by the intermediate bottom MoS<sub>2</sub> layer, and this situation would be preferable for achieving a strong PL intensity. This finding will be useful for controlling the optoelectronic properties of thick TMDCs and the demonstration of high-performance optoelectronic devices.

**Keywords:** transition metal dichalcogenide (TMDC); photoluminescence; superacid; molecular treatment; bilayer; molybdenum disulfide (MoS<sub>2</sub>)



**Citation:** Yamada, Y.; Yoshimura, T.; Ashida, A.; Fujimura, N.; Kiriya, D. Strong Photoluminescence Enhancement from Bilayer Molybdenum Disulfide via the Combination of UV Irradiation and Superacid Molecular Treatment. *Appl. Sci.* **2021**, *11*, 3530. <https://doi.org/10.3390/app11083530>

Academic Editor: Amerigo Beneduci

Received: 4 March 2021

Accepted: 7 April 2021

Published: 15 April 2021

**Publisher's Note:** MDPI stays neutral with regard to jurisdictional claims in published maps and institutional affiliations.



**Copyright:** © 2021 by the authors. Licensee MDPI, Basel, Switzerland. This article is an open access article distributed under the terms and conditions of the Creative Commons Attribution (CC BY) license (<https://creativecommons.org/licenses/by/4.0/>).

## 1. Introduction

Transition metal dichalcogenides (TMDCs) with a formula of MX<sub>2</sub> (M: Mo and W; X: S, Se, and Te) have garnered attention as atomically thin optoelectronic materials [1–4]. Various optical devices have been demonstrated, including phototransistors [5,6], photodetectors [7,8], valley-dependent optoelectronics [9–11], light-emitting diodes [12,13], and photovoltaics [14–16]. So far, monolayer (ML) TMDCs have been widely studied for application in optoelectronic devices because of their direct band gap nature at K and K' points in the Brillouin zone in the ML [17]. The layer-dependent electronic structure of TMDCs is well known, and the bilayer and thicker layered TMDCs show an indirect band gap nature [17,18]. The  $\Gamma$  point in the Brillouin zone increases with increasing the thickness, and both the conduction minimum and the K- $\Gamma$  points decrease with increasing the number of layers [17,18]. Photoluminescence (PL) shows clearly the difference in the electronic structure between ML and bilayer TMDCs [18]. In the case of a representative TMDC, MoS<sub>2</sub>, the ML shows a single PL spectrum around 1.9 eV corresponding to the direct band gap, while the bilayer shows two main peaks around 1.6 eV and 1.9 eV for the

coexistence of indirect and direct band gaps, respectively [18]. The PL intensity shown in the bilayer is usually very low compared with ML because of the dominant indirect band gap character.

Recently, chemical treatment on ML TMDCs has been reported, and a large enhancement of the PL intensity was demonstrated [19–23]. In the case of ML MoS<sub>2</sub>, treatment by oxidative chemicals such as tetracyanoquinodimethane [19] and quinone [20] derivatives, acids such as sulfuric acid [24], and hydrogen peroxide [25] show a large enhancement of the PL intensity. One of the strongest modulating agents of PL intensity in ML MoS<sub>2</sub> is a superacid molecule, bis(trifluoromethane)sulfonimide (TFSI), for both mechanically exfoliated and chemical-vapor-deposited ML flakes [26–30]. The PL enhancement mechanism is still under debate, but the existence of TFSI molecules on ML TMDC would be essential for achieving the strong PL intensity. Recently, we reported the consistent substantial PL enhancement of ML MoS<sub>2</sub> via a combination of TFSI treatment and additional UV irradiation [31]. In this work, we found an unusually strong PL enhancement from bilayer MoS<sub>2</sub> by combining the TFSI treatment with UV irradiation (Figures 1 and 2). The PL enhancement is over several hundred and some of them over 700× from the as-exfoliated bilayer flakes, and the shape of the PL spectrum dramatically changes to a sort of direct band gap. The plausible mechanism would be that the separation into a monolayer-like state would happen under the process. Furthermore, the indirect-to-direct band gap transition was only observed at the specific bilayer sample which would be like twisted bilayers. This work would facilitate controlling the interlayer interaction in TMDCs for modulating electronic structures to achieve atomically thin optoelectronic devices and physics platforms.

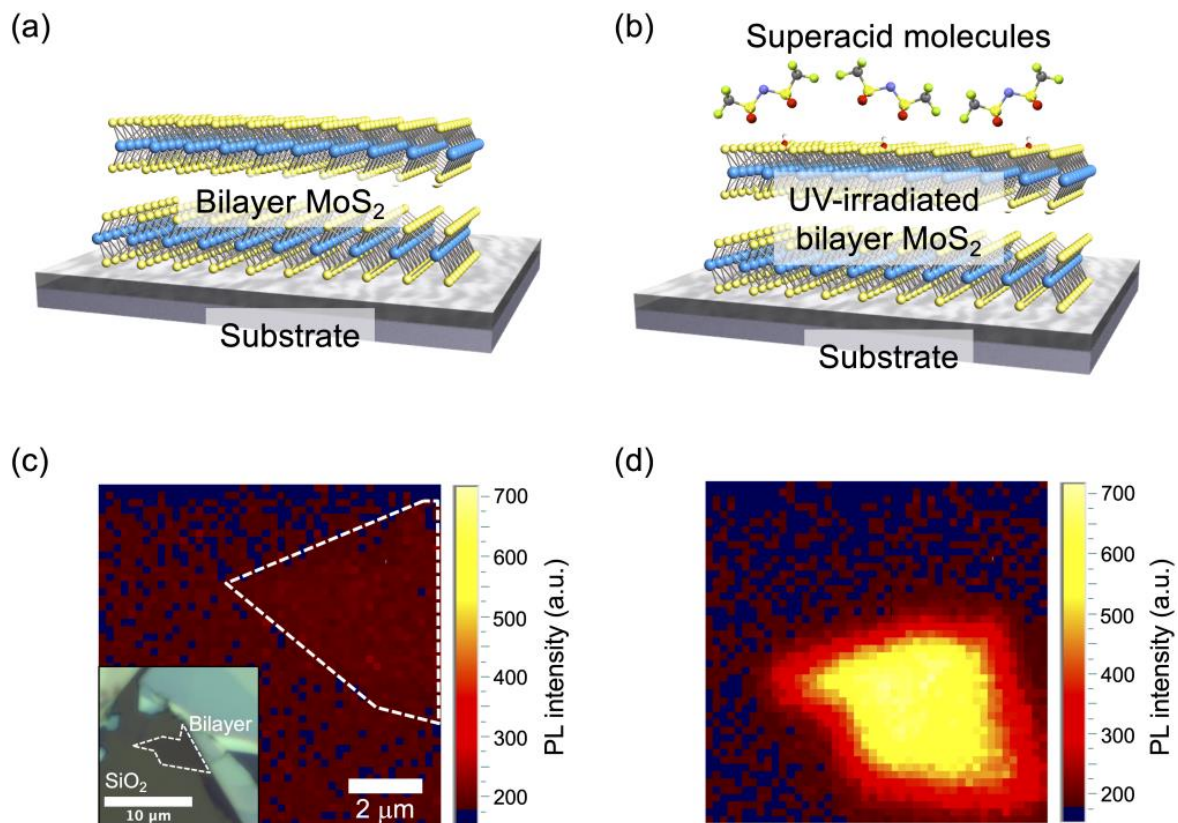


**Figure 1.** (a,b) Illustrative image of (a) the bilayer MoS<sub>2</sub> and (b) the bis(trifluoromethane)sulfonimide (TFSI) treatment for the UV-irradiated bilayer MoS<sub>2</sub>. (c,d) Photoluminescence (PL) mapping images for (c) the as-exfoliated bilayer MoS<sub>2</sub> and (d) the TFSI-treated sample for the UV-irradiated bilayer MoS<sub>2</sub>. The inset in Figure 1c is the optical microscope image for the targeted bilayer sample.

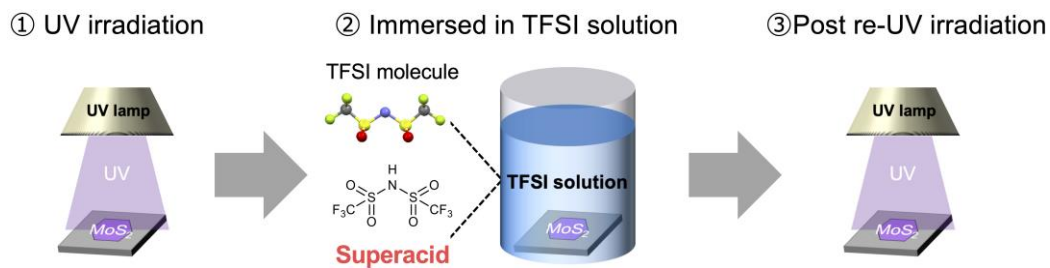


Figure 2. Illustrative image of the process applied to the bilayer MoS<sub>2</sub>.

## 2. Materials and Methods

Bulk MoS<sub>2</sub> was purchased from Structure Probe, Inc. (SPI Supplies). The bilayer flakes were prepared on Si wafer with 260 nm thermally grown SiO<sub>2</sub> (Silicon Valley Microelectronics, Inc.) via the mechanical exfoliation process. A weight ( $\sim 3.0 \text{ kg cm}^{-2}$ ) was used for the exfoliation process (Figures 1 and 3–5), pressing it over an exfoliation tape. In the case shown in Figure 6, the pressing weight was not applied. The TFSI molecule was purchased from Sigma-Aldrich, and acetonitrile (Kanto Chemical Co., Inc. Japan) was used as the solvent for the TFSI treatment. The TFSI solution ( $2 \text{ mg mL}^{-1}$ ) was prepared under an Ar atmosphere in a glove box (UNICO LTD. Japan, UL-1000A), and the TFSI treatment procedure was carried out in an ambient environment. The illustrative image of the process is shown in Figure 2. The UV irradiation process was performed for 5 min each (Figures 2–5). The exfoliated samples on the Si wafer were immersed in the solution at room temperature for 10 min in the normal treatment process (Figure 4). In the case shown in Figure 6, the total UV irradiation times were 15 min ( $5 \text{ min} \times 3$ ) for the initial UV irradiation procedure and 15 min ( $5 \text{ min} \times 3$ ) for the last repeated UV irradiation process to sufficiently modulate the bilayer sample. The lamp house (high-pressure mercury lamp,  $170 \text{ mW cm}^{-2}$ ) was placed 2 cm ( $\sim 4 \text{ cm}$  from the lamp) above the Si wafer. PL spectra were measured using a LabRAM HR800 equipped with an EMCCD camera (HORIBA Scientific, Japan). The wavelength was 532 nm for all measurements. The power of the incident beam was  $\sim 2.7 \text{ W cm}^{-2}$  for measurements of PL and Raman spectra in Figure 6b and  $27 \text{ W cm}^{-2}$  for other Raman spectra and PL mapping in Figure 1. Atomic force microscope (AFM) images were obtained using the dynamic force mode in SII instruments.

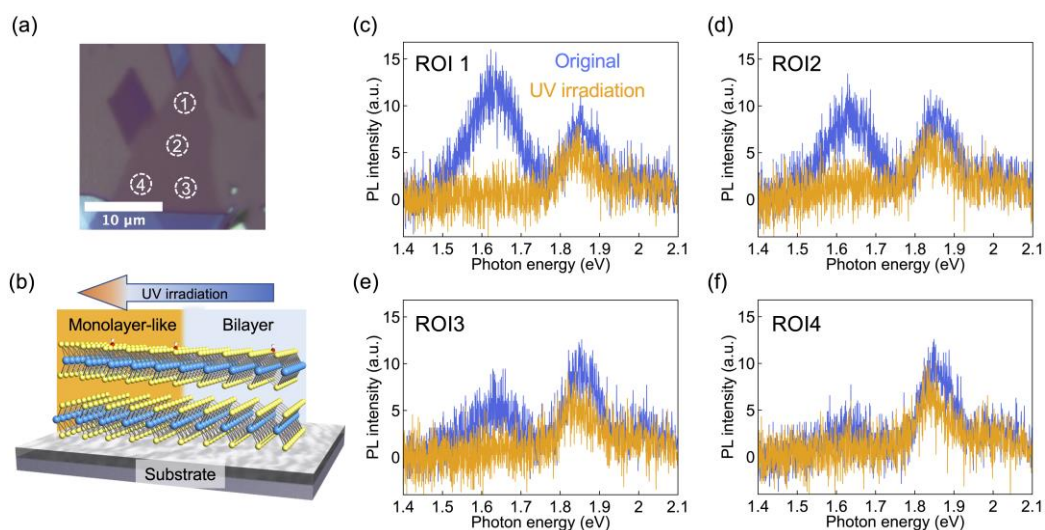
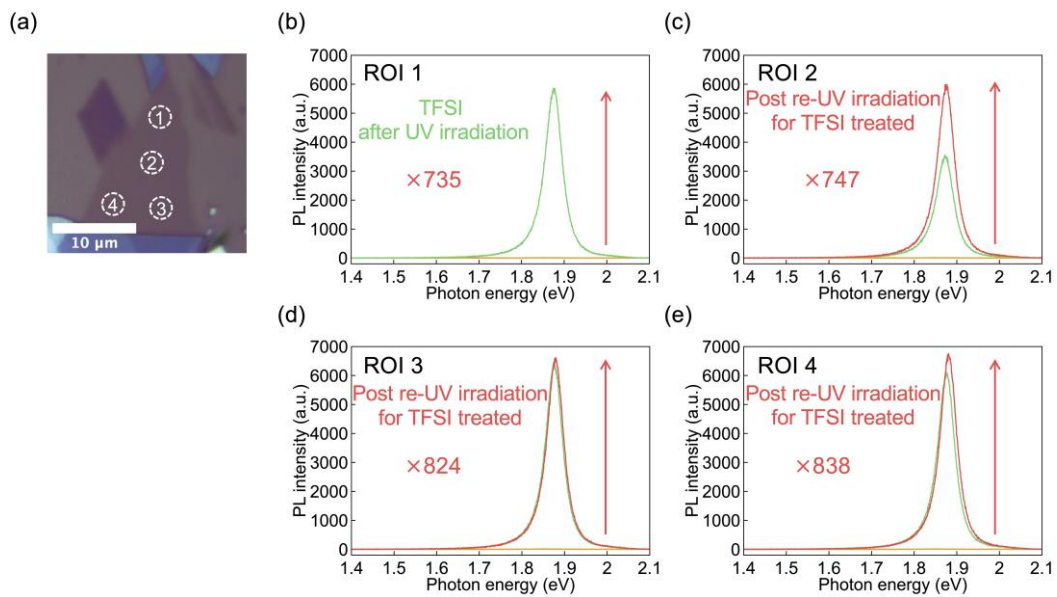
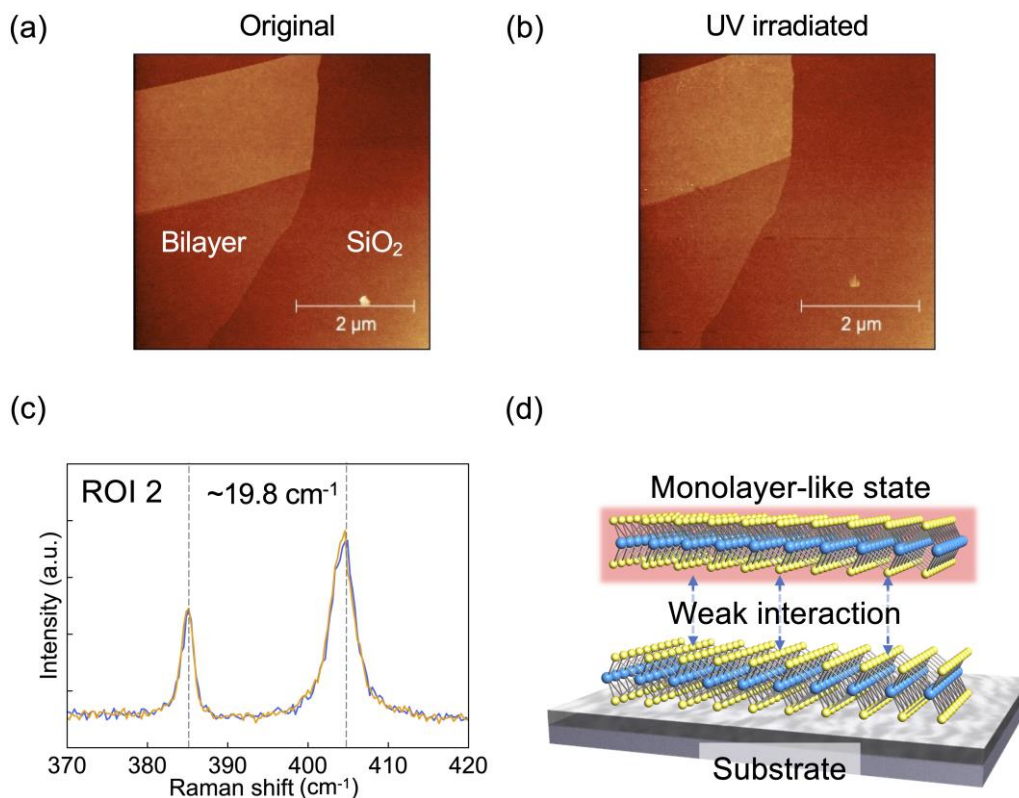


Figure 3. (a) Optical microscope image of the bilayer MoS<sub>2</sub>. The labels are the measurement regions (regions of interest (ROIs) 1–4) in Figure 3c–f. (b) Illustrative image of the modulation to the bilayer sample via the UV irradiation process. The process induces the bilayer to a monolayer-like state. (c–f) PL spectra for the as-exfoliated (original, blue) and the UV-irradiated (orange) samples in (c) ROI 1, (d) ROI 2, (e) ROI 3, and (f) ROI 4 in Figure 3a.



**Figure 4.** (a) Optical microscope image of the bilayer MoS<sub>2</sub> after the TFSI treatment followed by the UV irradiation. (b–e) PL spectra for the TFSI treatment (green) and the second (re-)UV irradiation (red) in (b) ROI 1, (c) ROI 2, (d) ROI 3, and (e) ROI 4 in Figure 4a. The values in Figure 4b–e are the magnitude of the PL enhancement in the sample over the as-exfoliated (original) sample.



**Figure 5.** (a,b) Atomic force microscope (AFM) images for (a) the as-exfoliated (original) bilayer MoS<sub>2</sub> exfoliated with the weight and (b) the UV-irradiated bilayer MoS<sub>2</sub>. (c) Raman spectra for the original (blue) and the UV-irradiated (orange) bilayer MoS<sub>2</sub> in ROI 2 in Figure 3. (d) Illustrative image of a plausible state of the bilayer MoS<sub>2</sub>. The top layer would show a monolayer-like state due to the weak interaction between the top and bottom layers by a sort of misalignment of each layer.

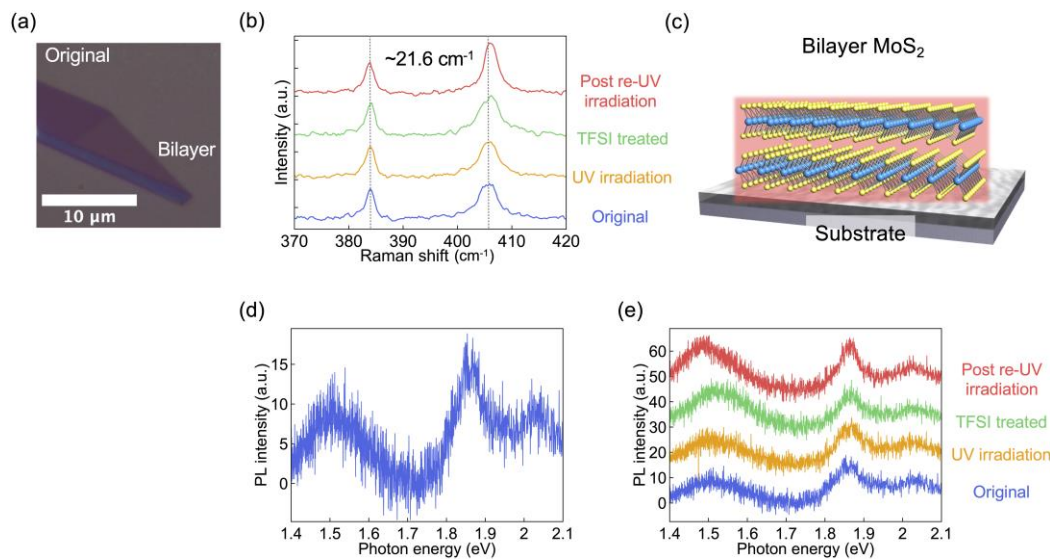


**Figure 6.** (a) Optical microscope image of the sample exfoliated without pressing with the weight. (b) Raman spectra for the as-exfoliated (original, blue), UV-irradiated (orange), TFSI-treated (green), and re-UV-irradiated (red) bilayer MoS<sub>2</sub>. The peak separation between E<sub>2g</sub> and A<sub>1g</sub> is about 21.6 cm<sup>-1</sup>. (c) The plausible situation of the bilayer MoS<sub>2</sub> from the Raman spectra in Figure 6b. This bilayer is a conventional flake. (d,e) PL spectra for the bilayer MoS<sub>2</sub> corresponds to Figure 6b; the original is shown in Figure 6d.

### 3. Results and Discussion

The sample targeted in this research is illustrated in Figure 1a,b. The bilayer MoS<sub>2</sub> flakes were prepared on the Si wafer covered with 260 nm SiO<sub>2</sub> via an exfoliation process. The flake was exfoliated with pressing the weight as shown in the experimental section. The TFSI molecular treatment was conducted along with the previously reported process; details are the combination of the UV irradiation and immersion into the TFSI acetonitrile solution [31]. Figure 1c,d show PL mapping images for the as-exfoliated and the processed bilayer MoS<sub>2</sub>, respectively. The bilayer MoS<sub>2</sub> shows a considerable PL enhancement, more than 100× around 1.9 eV, corresponding to a plausible direct band gap nature as seen in monolayers, via the TFSI molecular treatment with UV irradiation.

We examined each process for the PL enhancement of the bilayer MoS<sub>2</sub>. The UV irradiation process was carried out under an ambient condition, which may generate OH radicals on the surface of MoS<sub>2</sub> (Figure 3). In the previous work, an electronic structure of ML MoS<sub>2</sub> was maintained under UV irradiation, even while some chemical reactions happened on the surface [31,32]. Here, a laterally large (>10 μm) bilayer MoS<sub>2</sub> was applied to the UV irradiation process for 5 min; as a result, the whole area, regions of interest (ROIs) 1–4 in Figure 3, showed a more direct band gap nature with a single peak around 1.86 eV. The clear signal around 1.64 eV, corresponding to an indirect band gap, was diminished via the UV irradiation. According to the above result, UV irradiation would induce the separation of the top and bottom layers to achieve a ML-like state (Figure 3b).

We examined the ML-like sample with UV irradiation by further applying the TFSI treatment (Figure 4). This treatment changed the PL signal dramatically over the whole area (Figure 4b–e). All regions (ROIs 1–4) showed a direct band gap with a single PL signal around 1.88 eV by the TFSI treatment. The factor of the PL enhancement was over 700× from the as-exfoliated bilayer flakes. Therefore, the combination of UV irradiation and the TFSI treatment would be useful for modulating the optical property of bilayer MoS<sub>2</sub> to have a strong PL intensity like that of the TFSI-treated ML samples reported previously.

The supplemental UV irradiation was applied to the TFSI-treated bilayer MoS<sub>2</sub> but was found not to be so effective (re-UV irradiation for TFSI treated in Figure 4). This indicates that the combination of the first UV irradiation and the TFSI treatment process would achieve saturation of the PL enhancement. In the previous report, the UV irradiation

was applied after the TFSI treatment and was effective in enhancing the PL intensity for ML MoS<sub>2</sub> flakes [31]. We confirmed the same procedure as in the previous report for bilayer MoS<sub>2</sub>; a bilayer MoS<sub>2</sub> was treated first with TFSI solution, then by UV irradiation (Figure S1). The TFSI treatment itself changed the bilayer-like nature to a ML-like nature, but the PL intensity was still poor. The subsequent UV irradiation strongly enhanced the PL intensity, and the factor of the enhancement was several hundred times with a single signal around 1.9 eV. Therefore, the sequence of the TFSI treatment and the UV irradiation does not matter for achieving the PL enhancement; rather, the combination of both processes is the essence of obtaining the strong PL in the bilayer MoS<sub>2</sub> flakes.

Figure 5 shows atomic force microscope (AFM) images for the as-exfoliated (original) and UV-irradiated bilayer MoS<sub>2</sub>. The morphologies of bilayer MoS<sub>2</sub> maintain the structure via the UV irradiation process. Raman spectra for the sample maintain typical E<sub>2g</sub> and A<sub>1g</sub> modes for lateral and vertical vibration signals of MoS<sub>2</sub>. However, the peak separation of the two signals is less than 20 cm<sup>-1</sup>. In previous work, it was found that the peak separation of E<sub>2g</sub> and A<sub>1g</sub> modes is strongly dependent on the interlayer stacking of the bilayer, and the peak separation reduces if the bilayer is twisted [33–35]. We hypothesize that the bilayer sample might twist under the exfoliation process, because we pressed the exfoliation tape onto a substrate with a weight (~3.0 kg cm<sup>-2</sup>) when exfoliating the flake. MoS<sub>2</sub> is well known as a lubricant, and sliding between layers would happen with low friction [36]. This twisting would require more study in order to completely understand the situation. Importantly, the Raman signal is maintained after the UV irradiation process over the bilayer flake (Figure 5c and Figure S2), even though the character of the PL spectra converted from an indirect to a direct band gap nature, as shown in Figure 3.

The unusual event shown in the indirect-to-direct band gap conversion for the bilayer MoS<sub>2</sub> would be explained by the interlayer separation between the top and bottom layers (Figure 5d). Previously, a systematic study of twisted bilayer MoS<sub>2</sub> showed different PL and Raman signals [33–35]. By twisting the top and bottom layers, the peak separation of E<sub>2g</sub> and A<sub>1g</sub> reduces, as observed in our case. In addition, the peak position of the PL signal corresponding to the indirect band gap upshifts about 0.1 eV. Furthermore, the interlayer separation is also dependent on the interlayer stacking of the bilayer. If the bilayer is twisted, weak interaction between the top and bottom layers is expected. This scenario requires more study, but it would be a plausible explanation for the strong PL intensity from the bilayer MoS<sub>2</sub>. Another probable scenario to explain our observations would be etching the top layer and thinning it to a ML of MoS<sub>2</sub> via UV irradiation, because a laser-thinning process has been reported to reduce the thickness of MoS<sub>2</sub> [37–39]. However, the morphology and color of the sample are maintained in the process, as shown in Figure 5. It also would be hard to imagine the uniform etching of the whole region of the flake; therefore, we think the structure is maintained in the process.

To further confirm the process with a conventional, non-twisted bilayer MoS<sub>2</sub>. We prepared bilayer MoS<sub>2</sub> without using the weight simply by contacting bulk MoS<sub>2</sub> with a Si/SiO<sub>2</sub> wafer and exfoliating a bilayer flake (Figure 6a). The Raman spectrum showed E<sub>2g</sub> and A<sub>1g</sub> signals with a peak separation of 21.6 cm<sup>-1</sup>, corresponding to a typical (non-twisted) bilayer MoS<sub>2</sub> (Figure 6b,c) [19,40,41]. The PL measurement for the bilayer MoS<sub>2</sub> showed an indirect band gap around 1.5 eV and a direct band gap nature around 1.86 eV, respectively. The indirect band gap obtained without the weight showed a downshift from the bilayer signal exfoliated via pressing with the weight. These PL and Raman tendencies indicate a non-twisted bilayer MoS<sub>2</sub> via the exfoliation process without pressing with the weight. Then, the non-twisted bilayer flake was applied with the whole process of UV irradiation, TFSI treatment, and supplemental UV irradiation. Raman spectra showed almost no change in the process, even though the signal of the A<sub>1g</sub> showed a bit of an upshift because of the surface oxidation by the TFSI treatment. The PL signal also maintained the structure during the whole process. Therefore, the conventional, non-twisted bilayer flake did not show the conversion to a direct band gap. As in the above considerations, the observed direct band gap conversion in the bilayer MoS<sub>2</sub> would be a sort of separation of

the top and bottom layers. One explanation is that the conversion would happen in the twisted bilayer case because of the weak interaction between the top and bottom layers, and it facilitates the separation to the ML-like situation by the external perturbations.

#### 4. Conclusions

We demonstrated a substantial PL enhancement in the bilayer MoS<sub>2</sub>. The original bilayer MoS<sub>2</sub> showed a weak PL intensity with the signal of the indirect band gap. A key finding in this paper is that by both UV irradiation and TFSI treatment, the bilayer MoS<sub>2</sub> demonstrates a ML-like PL with a single signal at the direct band gap. In addition, the combined process induces more than several hundred times PL enhancement from the bilayer MoS<sub>2</sub> compared to the as-exfoliated bilayer flakes. The enhancement mechanism requires more study, but it would involve the separation of the top and bottom layers in the bilayer MoS<sub>2</sub>. This situation would be due to a sort of misalignment of the top and bottom layers caused by pressing the weight and sliding each layer in the exfoliation process. If the bilayer is twisted, the interlayer separation between the top and bottom layers would happen easily, which would lead to an indirect-to-direct band gap conversion via the process. These phenomena are also supported by treating a conventional bilayer MoS<sub>2</sub> flake; there is no PL enhancement in the conventional case. This technique is useful for preparing high-optical-quality MoS<sub>2</sub> materials and devices. Since the sample is bilayer, the top layer is separated from the substrate; the bottom MoS<sub>2</sub> layer would serve as an interface layer between the top layer with a strong PL and the substrate. This structure would be effective in removing substrate effects. This work would open another strategy to obtain a strong PL intensity from 2D materials and be useful in optical device applications.

**Supplementary Materials:** The following are available online at <https://www.mdpi.com/article/10.3390/app11083530/s1>, Figure S1: PL enhancement via the process of TFSI treatment followed by UV irradiation for the bilayer MoS<sub>2</sub> and Figure S2: Raman spectra for the UV-irradiated bilayer MoS<sub>2</sub>.

**Author Contributions:** Conducted all experiments, Y.Y.; designed the experiments and wrote the manuscript, Y.Y. and D.K. All authors discussed continuously and contributed to the writing of the manuscript. All authors have read and agreed to the published version of the manuscript.

**Funding:** This research was funded by JSPS KAKENHI (20H02574), the Research Foundation for Opto-Science and Technology, the Konica Minolta Science and Technology Foundation, and the Sumitomo Foundation.

**Institutional Review Board Statement:** This project does not include biological items requiring ethical approval.

**Informed Consent Statement:** It is not required.

**Data Availability Statement:** The study data is available from the corresponding author on request.

**Conflicts of Interest:** The authors declare no conflict of interest.

#### References

1. Wang, Q.H.; Kalantar-Zadeh, K.; Kis, A.; Coleman, J.N.; Strano, M.S. Electronics and optoelectronics of two-dimensional transition metal dichalcogenides. *Nat. Nanotechnol.* **2012**, *7*, 699. [[CrossRef](#)]
2. Chhowalla, M.; Shin, H.S.; Eda, G.; Li, L.J.; Loh, K.P.; Zhang, H. The chemistry of two-dimensional layered transition metal dichalcogenide nanosheets. *Nat. Chem.* **2013**, *5*, 263. [[CrossRef](#)] [[PubMed](#)]
3. Geim, A.K.; Grigorieva, I.V. Van der Waals heterostructures. *Nature* **2013**, *499*, 419. [[CrossRef](#)] [[PubMed](#)]
4. Jariwala, D.; Sangwan, V.K.; Lauhon, L.J.; Marks, T.J.; Hersam, M.C. Emerging device applications for semiconducting two-dimensional transition metal dichalcogenides. *ACS Nano* **2014**, *8*, 1102. [[CrossRef](#)] [[PubMed](#)]
5. Lee, H.S.; Min, S.W.; Chang, Y.G.; Park, M.K.; Nam, T.; Kim, H.; Kim, J.H.; Ryu, S.; Im, S. MoS<sub>2</sub> nanosheet phototransistors with thickness-modulated optical energy gap. *Nano Lett.* **2012**, *12*, 3695. [[CrossRef](#)] [[PubMed](#)]
6. Yin, Z.; Li, H.; Li, H.; Jiang, L.; Shi, Y.; Sun, Y.; Lu, G.; Zhang, Q.; Chen, X.; Zhang, H. Single-Layer MoS<sub>2</sub> Phototransistors. *ACS Nano* **2012**, *6*, 74. [[CrossRef](#)] [[PubMed](#)]
7. Wang, X.; Wang, P.; Wang, J.; Hu, W.; Zhou, X.; Guo, N.; Huang, H.; Sun, S.; Shen, H.; Lin, T.; et al. Ultrasensitive and Broadband MoS<sub>2</sub> Photodetector Driven by Ferroelectrics. *Adv. Mater.* **2015**, *27*, 6575. [[CrossRef](#)]

8. Lopez-Sanchez, O.; Lembke, D.; Kayci, M.; Radenovic, A.; Kis, A. Ultrasensitive photodetectors based on monolayer MoS<sub>2</sub>. *Nat. Nanotechnol.* **2013**, *8*, 497. [[CrossRef](#)]
9. Mak, K.F.; He, K.; Shan, J.; Heinz, T.F. Control of valley polarization in monolayer MoS<sub>2</sub> by optical helicity. *Nat. Nanotechnol.* **2012**, *7*, 494. [[CrossRef](#)]
10. Zeng, H.; Dai, J.; Yao, W.; Xiao, D.; Cui, X. Valley polarization in MoS<sub>2</sub> monolayers by optical pumping. *Nat. Nanotechnol.* **2012**, *7*, 490. [[CrossRef](#)]
11. Onga, M.; Zhang, Y.; Ideue, T.; Iwasa, Y. Exciton Hall effect in monolayer MoS<sub>2</sub>. *Nat. Mater.* **2017**, *16*, 1193. [[CrossRef](#)] [[PubMed](#)]
12. Ross, J.S.; Klement, P.; Jones, A.M.; Ghimire, N.J.; Yan, J.; Mandrus, D.G.; Taniguchi, T.; Watanabe, K.; Kitamura, K.; Yao, W.; et al. Electrically tunable excitonic light-emitting diodes based on monolayer WSe<sub>2</sub> p–n junctions. *Nat. Nanotechnol.* **2014**, *9*, 268. [[CrossRef](#)] [[PubMed](#)]
13. Lien, D.-H.; Amani, M.; Desai, S.B.; Ahn, G.H.; Han, K.; He, J.-H.; Ager, J.W.; Wu, M.C.; Javey, A. Large-area and bright pulsed electroluminescence in monolayer semiconductors. *Nat. Commun.* **2018**, *9*, 1229. [[CrossRef](#)] [[PubMed](#)]
14. Wong, J.; Jariwala, D.; Tagliabue, G.; Tat, K.; Davoyan, A.R.; Sherrott, M.C.; Atwater, H.A. High Photovoltaic Quantum Efficiency in Ultrathin van der Waals Heterostructures. *ACS Nano* **2017**, *11*, 7230. [[CrossRef](#)] [[PubMed](#)]
15. Tsai, M.-L.; Su, S.-H.; Chang, J.-K.; Tsai, D.-S.; Chen, C.-H.; Wu, C.-I.; Li, L.-J.; Chen, L.-J.; He, J.-H. Monolayer MoS<sub>2</sub> Heterojunction Solar Cells. *ACS Nano* **2014**, *8*, 8317. [[CrossRef](#)]
16. Tsai, M.-L.; Li, M.-Y.; Retamal JR, D.; Lam, K.-T.; Lin, Y.-C.; Suenaga, K.; Chen, L.-J.; Liang, G.; Li, L.-J.; He, J.-H. Single Atomically Sharp Lateral Monolayer p–n Heterojunction Solar Cells with Extraordinarily High Power Conversion Efficiency. *Adv. Mater.* **2017**, *29*, 1701168. [[CrossRef](#)]
17. Splendiani, A.; Sun, L.; Zhang, Y.; Li, T.; Kim, J.; Chim, C.-Y.; Galli, G.; Wang, F. Emerging Photoluminescence in Monolayer MoS<sub>2</sub>. *Nano Lett.* **2010**, *10*, 1271–1275. [[CrossRef](#)] [[PubMed](#)]
18. Mak, K.F.; Lee, C.; Hone, J.; Shan, J.; Heinz, T.F. Atomically Thin MoS<sub>2</sub>: A New Direct-Gap Semiconductor. *Phys. Rev. Lett.* **2010**, *105*, 136805. [[CrossRef](#)]
19. Mouri, S.; Miyauchi, Y.; Matsuda, K. Tunable photoluminescence of monolayer MoS<sub>2</sub> via chemical doping. *Nano Lett.* **2013**, *13*, 5944–5948. [[CrossRef](#)]
20. Ichimiya, H.; Fukui, A.; Aoki, Y.; Yamada, Y.; Yoshimura, T.; Ashida, A.; Fujimura, N.; Kiriya, D. Solvent engineering for strong photoluminescence enhancement of monolayer molybdenum disulfide in redox-active molecular treatment. *Appl. Phys. Exp.* **2019**, *12*, 051014. [[CrossRef](#)]
21. Yao, H.; Liu, L.; Wang, Z.; Li, H.; Chen, L.; Pam, M.E.; Chen, W.; Yang, H.Y.; Zhang, W.; Shi, Y. Significant photoluminescence enhancement in WS<sub>2</sub> monolayers through Na<sub>2</sub>S treatment. *Nanoscale* **2018**, *10*, 6105–6112. [[CrossRef](#)]
22. Han, H.V.; Lu, A.Y.; Lu, L.S.; Huang, J.K.; Li, H.; Hsu, C.L.; Lin, Y.C.; Chiu, M.H.; Suenaga, K.; Chu, C.W.; et al. Photoluminescence enhancement and structure repairing of monolayer MoSe<sub>2</sub> by hydrohalic acid treatment. *ACS Nano* **2016**, *10*, 1454–1461. [[CrossRef](#)]
23. Tanoh AO, A.; Alexander-Webbe, J.; Xiao, J.; Delport, G.; Williams, C.A.; Bretscher, H.; Gauriot, N.; Allardice, J.; Pandya, R.; Fan, Y.; et al. Enhancing Photoluminescence and Mobilities in WS<sub>2</sub> Monolayers with Oleic Acid Ligands. *Nano Lett.* **2019**, *19*, 6299–6307. [[CrossRef](#)] [[PubMed](#)]
24. Kiriya, D.; Hijikata, Y.; Pirillo, J.; Kitaura, R.; Murai, A.; Ashida, A.; Yoshimura, T.; Fujimura, N. Systematic Study of Photoluminescence Enhancement in Monolayer Molybdenum Disulfide by Acid Treatment. *Langmuir* **2018**, *34*, 10243–10249. [[CrossRef](#)] [[PubMed](#)]
25. Su, W.; Dou, H.; Li, J.; Huo, D.; Dai, N.; Yang, L. Tuning photoluminescence of single-layer MoS<sub>2</sub> using H<sub>2</sub>O<sub>2</sub>. *RSC Adv.* **2015**, *5*, 82924. [[CrossRef](#)]
26. Amani, M.; Taheri, P.; Addou, R.; Ahn, G.H.; Kiriya, D.; Lien, D.H.; Ager, J.W.; Wallace, R.M.; Javey, A. Recombination Kinetics and Effects of Superacid Treatment in Sulfur- and Selenium-Based Transition Metal Dichalcogenides. *Nano Lett.* **2016**, *16*, 2786–2791. [[CrossRef](#)] [[PubMed](#)]
27. Amani, M.; Burke, R.A.; Ji, X.; Zhao, P.; Lien, D.H.; Taheri, P.; Ahn, G.H.; Kirya, D.; Ager, J.W.; Yablonoitch, E.; et al. High Luminescence Efficiency in MoS<sub>2</sub> Grown by Chemical Vapor Deposition. *ACS Nano* **2016**, *10*, 6535–6541. [[CrossRef](#)]
28. Kim, H.; Lien, D.H.; Amani, M.; Ager, J.W.; Javey, A. Highly Stable Near-Unity Photoluminescence Yield in Monolayer MoS<sub>2</sub> by Fluoropolymer Encapsulation and Superacid Treatment. *ACS Nano* **2017**, *11*, 5179–5185. [[CrossRef](#)]
29. Cadiz, F.; Tricard, S.; Gay, M.; Lagarde, D.; Wang, G.; Robert, C.; Renucci, P.; Urbaszek, B.; Marie, X. Well separated trion and neutral excitons on superacid treated MoS<sub>2</sub> monolayers. *Appl. Phys. Lett.* **2016**, *108*, 251106. [[CrossRef](#)]
30. Zeng, Y.; Chen, W.; Tang, B.; Liao, J.; Lou, J.; Chen, Q. Synergetic photoluminescence enhancement of monolayer MoS<sub>2</sub>: Via surface plasmon resonance and defect repair. *RSC Adv.* **2018**, *8*, 23591–23598. [[CrossRef](#)]
31. Yamada, Y.; Shinokita, K.; Okajima, Y.; Takeda, S.N.; Matsushita, Y.; Takei, K.; Yoshimura, T.; Ashida, A.; Fujimura, N.; Matsuda, K.; et al. Photoactivation of Strong Photoluminescence in Superacid-Treated Monolayer Molybdenum Disulfide. *ACS Appl. Mater. Interfaces* **2020**, *12*, 36496–36504. [[CrossRef](#)]
32. Details are shown on a submitted manuscript. Under review.
33. Huang, S.; Liang, L.; Ling, X.; Puzetky, A.A.; Geohegan, D.B.; Sumpter, B.G.; Kong, J.; Meunier, V.; Dresselhaus, M.S. Low-Frequency Interlayer Raman Modes to Probe Interface of Twisted Bilayer MoS<sub>2</sub>. *Nano Lett.* **2016**, *16*, 1435–1444. [[CrossRef](#)] [[PubMed](#)]

34. Liu, K.; Zhang, L.; Cao, T.; Jin, C.; Qiu, D.; Zhou, Q.; Zettl, A.; Yang, P.; Louie, S.G.; Wang, F. Evolution of interlayer coupling in twisted molybdenum disulfide bilayers. *Nat. Commun.* **2014**, *5*, 4966. [[CrossRef](#)]
35. Liao, M.; Wei, Z.; Du, L.; Wang, Q.; Tang, J.; Yu, H.; Wu, F.; Zhao, J.; Xu, X.; Han, B.; et al. Precise control of the interlayer twist angle in large scale MoS<sub>2</sub> homostructures. *Nat. Commun.* **2020**, *11*, 2153. [[CrossRef](#)] [[PubMed](#)]
36. Li, H.; Wang, J.; Gao, S.; Chen, Q.; Peng, L.; Liu, K.; Wei, X. Superlubricity between MoS<sub>2</sub> Monolayers. *Adv. Mater.* **2017**, *29*, 1701474. [[CrossRef](#)] [[PubMed](#)]
37. Hu, L.; Shan, X.; Wu, Y.; Zhao, J.; Lu, X. Laser Thinning and Patterning of MoS<sub>2</sub> with Layer-by-Layer Precision. *Sci. Rep.* **2017**, *7*, 15538. [[CrossRef](#)] [[PubMed](#)]
38. Kim, H.-J.; Yun, Y.J.; Yi, S.N.; Chang, S.K.; Ha, D.H. Changes in the Photoluminescence of Monolayer and Bilayer Molybdenum Disulfide during Laser Irradiation. *ACS Omega* **2020**, *5*, 7903. [[CrossRef](#)] [[PubMed](#)]
39. Tessarek, C.; Gridenco, O.; Wiesing, M.; Müssener, J.; Figge, S.; Sebald, K.; Gutowski, J.; Eickhoff, M. Controlled Laser-Thinning of MoS<sub>2</sub> Nanolayers and Transformation to Amorphous MoO<sub>x</sub> for 2D Monolayer Fabrication. *ACS Appl. Nano Mater.* **2020**, *3*, 7490–7498. [[CrossRef](#)]
40. Niu, Y.; Gonzalez-Abad, S.; Frisenda, R.; Marauhn, P.; Drüppel, M.; Gant, P.; Schmidt, R.; Taghavi, N.S.; Barcons, D.; Molina-Mendoza, A.J.; et al. Thickness-Dependent Differential Reflectance Spectra of Monolayer and Few-Layer MoS<sub>2</sub>, MoSe<sub>2</sub>, WS<sub>2</sub> and WSe<sub>2</sub>. *Nanomaterials* **2018**, *8*, 725. [[CrossRef](#)]
41. Lee, C.; Yan, H.; Brus, L.E.; Heinz, T.F.; Hone, J.; Ryu, S. Anomalous Lattice Vibrations of Single- and Few-Layer MoS<sub>2</sub>. *ACS Nano* **2010**, *4*, 2695. [[CrossRef](#)]